Journal of the European Ceramic Society 41 (2021) 1530–1536

Contents lists available at ScienceDirect

Journal of the European Ceramic Society

journal homepage: www.elsevier.com/locate/jeurceramsoc

Original article

Enhanced methylene blue removal efficiency of TiO_2 embedded porous glass

E. Burak Ertuş [a], Cekdar Vakifahmetoglu [b,*], Abdullah Öztürk [c]

[a] KTO Karatay University, Department of Mechanical Engineering, Konya, Turkey
[b] İzmir Institute of Technology, Department of Materials Science and Engineering, İzmir, Turkey
[c] Middle East Technical University, Department of Metallurgical and Materials Engineering, Ankara, Turkey

ARTICLE INFO

Keywords:
Porous glass
Titanium dioxide
Leaching
Methylene blue
Photocatalysis

ABSTRACT

A porous glass (PG) embedded with titanium dioxide (TiO_2) was produced via impregnation of the PG with Titanium (IV) Isopropoxide solution followed by crystallization. N_2 sorption analyses revealed that the specific surface area (SSA) and total pore volume of the PG reached to 358 m^2/g and 0.370 cm^3/g, respectively. The adsorption capacity of methylene blue (MB) for the glasses was measured in the dark, instead the photocatalytic MB removal efficiency was evaluated by the degradation of MB under UV light illumination using a UV–vis spectrometer. The MB removal efficiency of the TiO_2 synthesized anatase powder was only 32.3 % whereas, for TiO_2 embedded PG (TiPG) it was 91.6 %, and nearly complete (> 99 %) efficacy was achieved for TiO_2 embedded alkaline leached PG (TiPG-AL) under UV illumination 3 h period. Better MB removal efficiency was attributed to high SSA and dispersion of nano size anatase TiO_2 crystallites within the porous structure.

1. Introduction

Titanium dioxide (TiO_2) based photocatalytic systems have attracted great attention for pollutant removal applications because they offer high conversion efficiency, good chemical/photo stability, and low cost [1,2]. In the simplest system, TiO_2 powders are used in a suspension for purification of contaminated aqueous solutions; e.g. wastewater [1,3]. However, fine powders in slurry systems tend to agglomerate and reduce reactive surface sites [4]. Additionally, the effected TiO_2 particles must be separated by additional filtration processes [5]. Though TiO_2 coating has been applied as a remedy to those difficulties, surface detachment and restricted effective surface area still remain as drawbacks [6,7]. Lately, studies focusing on the development of TiO_2 embedded porous substrates such as silica [8,9], mesoporous silica [10], carbon [11,12], SiC [13,14], Al_2O_3 [15], and porous glass (PG) [16–18] have shown encouraging outcomes. PGs offer unique sponge-like interconnected porous structure, high optical transparency, and mechanical integrity [19,20]. Pore topology, size, volume thus, the surface area can be tailored via processing route [19]. PGs are manufactured in various forms such as monoliths, beads, plates, fibers/rods/tubes, and they could be used as optical chemo-sensor, membrane, drug delivery systems, etc. [21–24].

Considering that PG has already been used as an effective adsorbent [25], an understanding on the preparation and photocatalytic properties of TiO_2 embedded PG could extend its utilization in special photocatalytic applications including air and wastewater purification through a synergic purification effect coming from both adsorption and photocatalysis. It has been also noted that the PG substrate can prevent the catalyst poisoning [26,27]. Accordingly, the aim of this investigation was to produce and evaluate the adsorption and photocatalytic properties of anatase TiO_2 embedded PG by using methylene blue (MB) dye, such economic monoliths with long term photostability is anticipated to be used in indoor air and wastewater purification systems.

2. Experimental procedure

2.1. Sample preparation

The porous glass samples were produced according to the previously published results [28]. Simply, a sodium borosilicate glass (SBG) with nominal composition of $55.7SiO_2$-$33.6B_2O_3$-$9.2Na_2O$-$1.5Al_2O_3$ (wt %) was produced by conventional melt-quenching method. Then, the SBG pieces were heat treated at 500 °C for 9 h to induce the phase separation. After that, the heat treated glass pieces were first acid leached using 1 M

* Corresponding author.
E-mail address: cekdarvakifahmetoglu@iyte.edu.tr (C. Vakifahmetoglu).

https://doi.org/10.1016/j.jeurceramsoc.2020.09.047
Received 5 August 2020; Received in revised form 18 September 2020; Accepted 21 September 2020
Available online 23 September 2020

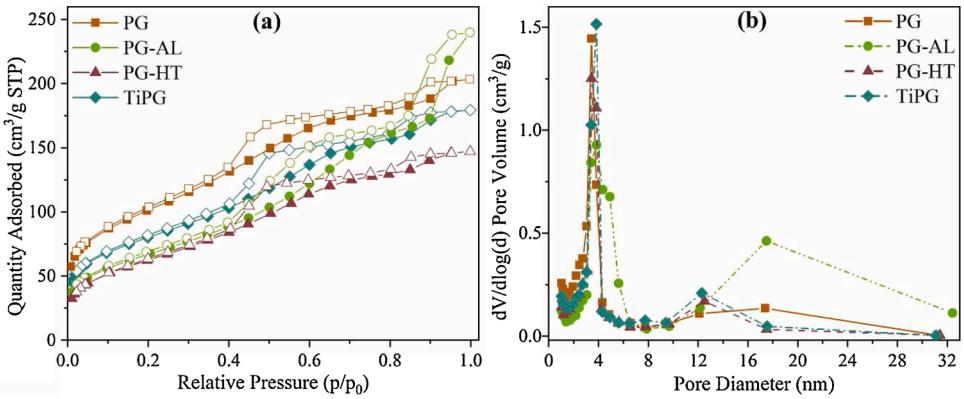

Fig. 1. **(a)** N_2 adsorption-desorption isotherms, and **(b)** pore size distribution data for porous glasses.

HCl solution at 80 °C for 24 h. In order to remove the silica clusters remained in the liquation channels, the acid leached porous glass (PG) was additionally alkaline leached using 0.5 M NaOH solution at room temperature (RT) for 2 h to get PG-AL. In separate experiments, additional heat treatment was conducted on PG at 800 °C for 1 h to obtain heat treated PG (PG-HT). These alterations were followed to induce different pore architecture, surface functionality and their effect on the resulting MB adsorption and photocatalytic properties.

Different PGs produced were used as substrates for the growth of TiO_2 crystallites within the porous structure. 1 M Titanium (IV) Isopropoxide (TTIP, analytical grade, Sigma-Aldrich, Darmstadt, Germany)/isopropyl alcohol solution was employed as titanium (Ti) precursor. PG monoliths of approximately 1.5 mm thickness were immersed in the TTIP solution at RT for 24 h while stirring at 900 rpm. When the impregnation was completed, the monoliths were degassed for 1 h, let for hydrolysis reactions (24 h at ambient conditions), followed by dying, and heat treatment at 450 °C for 4 h in air for TiO_2 crystallization.

Titanium impregnated PGs were named by adding Ti in front of the substrate name used for embedding (e.g. Ti impregnated PG was named as TiPG). For the purpose of comparison, TiPG was re-immersed in the same TTIP solution at the same conditions to get twice Ti impregnated PG (Tix2PG). In addition, TiO_2 powder was separately synthesized by using the same chemicals and procedure applied to obtain TiO_2 embedded PGs. A 0.01 g of TiO_2 powder which was assumed equal to the weight gain measured for PG after Ti-impregnation and heat treatment causing crystallization, was used in the decolorization tests for comparative assessment.

2.2. Characterization

The pore morphologies developed in different PGs were evaluated by nitrogen (N_2) sorption test using Quantachrome Autosorb-6 (Boynton Beach, Florida, USA). Prior to the measurements, the samples were degassed at 200 °C for 3 h. The specific surface area (SSA) was calculated using Brunauer–Emmett–Teller (BET) equation from the adsorption isotherm. The total pore volume (V_P) was calculated from the amount of gas adsorbed at the relative pressure P/P_0 of 0.99. The pore size distribution was determined from the desorption branch of the N_2 sorption hysteresis according to the Barrett–Joyner–Halenda (BJH) method, based on the Kelvin equation, which relates the pore size with critical condensation pressure assuming a straight cylindrical pore model [29].

The crystalline phases developed in TiPGs were identified using an X-ray diffractometer (XRD, Bruker-AXS, D8 Advance A25, Germany). XRD scans were collected using CuK_α radiation ($\lambda = 1.54056$ Å) between 2θ of 10 and 90° at a scanning rate of 0.2°/min. The Fourier Transform Infrared transmission spectra of the PGs were measured using a FTIR spectrometer (PerkinElmer Frontier, Waltham MA, USA) instrument equipped with ATR (Gladi, Pike Technology, Madison, Wisconsin, USA) apparatus in the range of 400–4000 cm^{-1} with a resolution of 1 cm^{-1}. A linear baseline was first fitted to the IR spectra then normalized to signal intensity.

The structure of the pores and the microstructures of the crystalline phases were examined using a scanning electron microscope (FE-SEM, Nova Nanosem 430, Hillsboro OR, USA). An energy dispersive spectroscopy (EDS) attached to FESEM was employed to define the elemental composition of PGs. The impregnated surface of TiPG was coated with approximately 10 nm layer of gold using a sputter coater (Quorum SC7640, Ashford, United Kingdom) prior to FESEM examination. The transmission spectra of PGs and TiPGs were measured in the wavelength range from 250 to 850 nm with a step of 1 nm using a UV–vis spectrometer (Scinco S-3100, Seoul, S. Korea). The optical band gap energy (Eg) values of the samples were measured using UV–vis diffuse reflectance spectra. The reflectance (R) data was converted to the F(R) values using the Kubelka–Munk equation given in Eq. (1). Then, $(F(R)h\nu)^{1/2}$ against $h\nu$ (eV) graph was plotted and Eg for indirect transition was calculated by extrapolating the midsection of the graph to the $h\nu$ axis [30].

$$F(R)_{KM} = (1\text{-}R)^2 / 2R \quad (1)$$

The MB adsorption capacity in the dark and the MB photocatalytic removal efficiency under UV light illumination for selected PGs and TiPGs were evaluated by the change of MB concentration (10 ppm) in the solution during the experiments performed using 30 mL MB-distilled (DI) water solution (at a pH of 5.6) in a 250 mL glass container. Selected glass chunks with a thickness of 1.5 mm and a total weight of 0.3 g were horizontally placed into glass container. The MB concentration change was defined as the absorbance of the solution at a wavelength of 664 nm. 3 mL of the solution was periodically taken and analyzed using a UV–vis spectrometer (Scinco S-3100, Seoul S. Korea). All initial adsorption tests were carried out under continuous stirring (~500 rpm) in a complete dark environment. For the total removal efficiency analysis under UV irritation, TiO_2 embedded samples (TiPGs) were placed in MB solutions and irradiated simultaneously by a 100 W UV lamp (UVP, Blak-Ray, San Gabriel CA, USA) with a wavelength at 365 nm. The removal efficiency (RE) of the glasses was calculated using Eq. (2). Where; C_0 and C_t are the concentrations of MB at initial and different irradiation times, respectively. Each glass specimen was tested three times. The data points were calculated by taking the mean values and standard deviations of three different representative specimens for each glass.

$$RE = \frac{(C_0\text{-}C_t)}{C_0} * 100 \quad (2)$$

3. Results and discussion

3.1. Structural analysis

The N_2 sorption isotherms for PG, PG-AL, PG-HT, and TiPG are

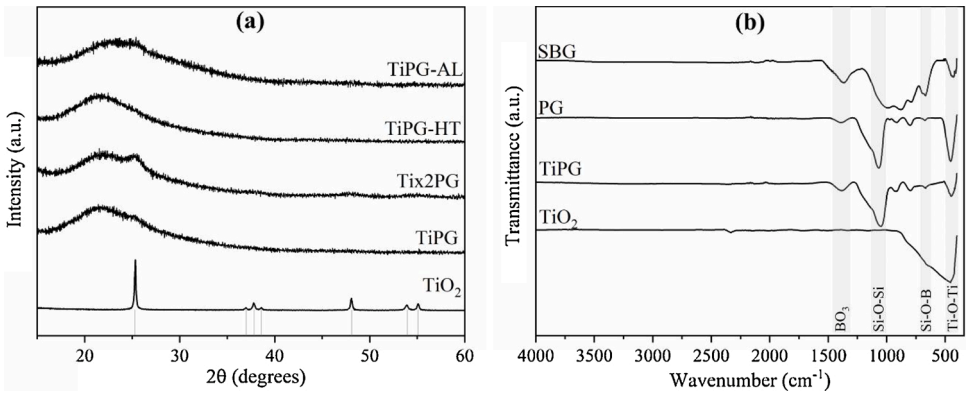

Fig. 2. Normalized; **(a)** XRD patterns for TiPG-AL, TiPG-HT, Tix2PG, TiPG, and TiO_2 powder, and **(b)** FTIR spectra for SBG, PG, TiPG, and TiO_2.

shown in Fig. 1**(a)**. The hysteresis loops in the Type IV(a) isotherms according to the IUPAC classifications [29], indicated that all glasses contain mesoporosity. The microporosity is not clearly visible from the pore size distribution curves shown in Fig. 1**(b)**. But the steep increase in the adsorption at very low relative pressures shown in Fig. 1**(a)**, suggests that all PGs contain hierarchical porosity (both micro and meso porosity) particularly gradient porosity in the mesoporosity range. The specific surface area (SSA) and the pore volume (Vp) values calculated for PG, PG-AL, PG-HT were 358.0, 241.2, 228.4 m^2/g, and 0.314, 0.370, 0.227 cm^3/g, respectively.

In general, for porous glasses produced via acid etching, the pores generated around 5 nm are associated with the inter-particle spaces in between the channel walls and silica clusters (themselves as well). Instead, the larger mesopores evolving in a broader range up to 35 nm are related with the so called "liquation channels" [31,32]. When subsequent alkaline leaching was performed on PG, the size of the pores in

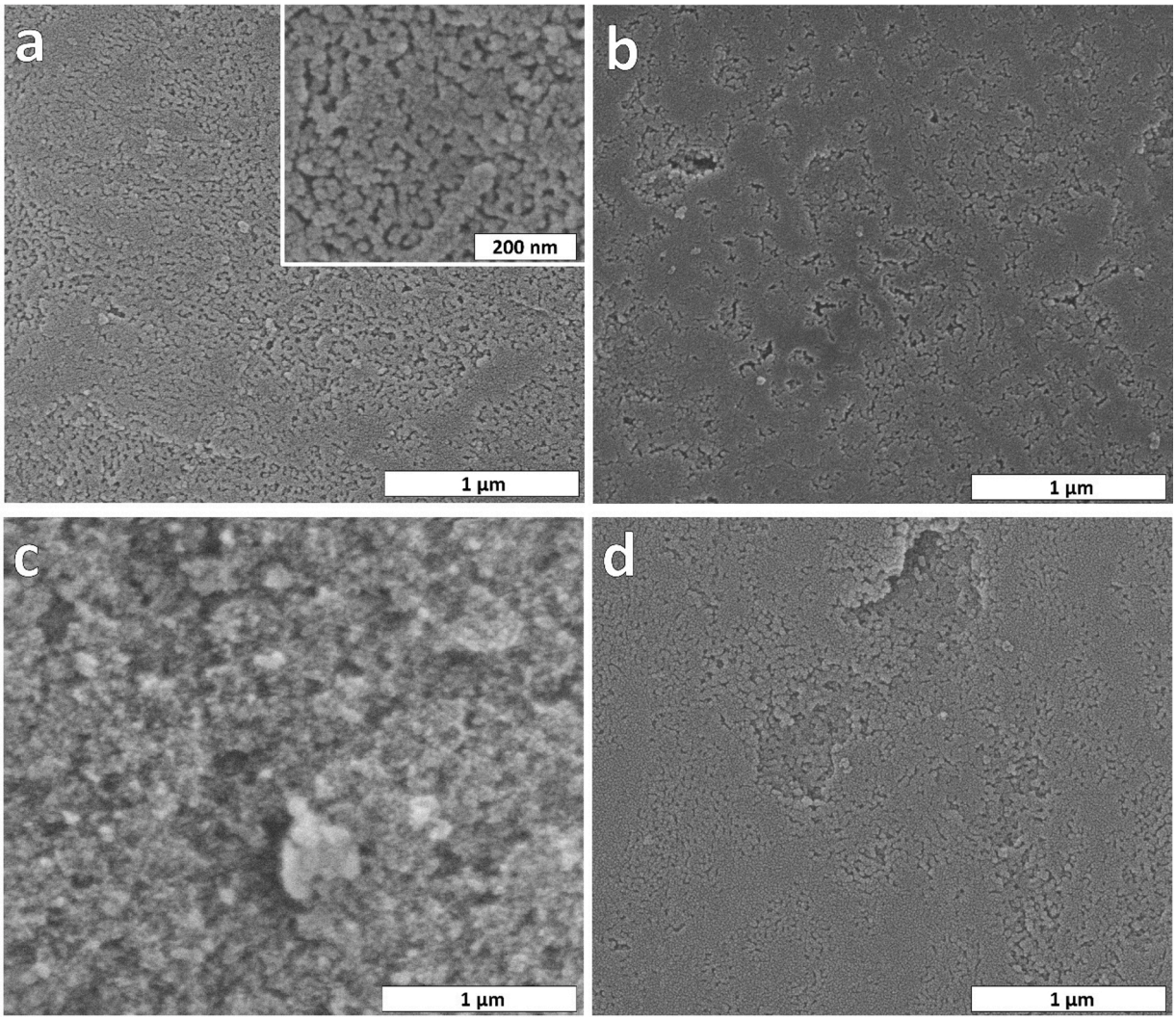

Fig. 3. SEM images taken from the surfaces of **(a)** TiPG, **(b)** Tix2PG, **(c)** TiPG-AL, and **(d)** TiPG-HT.

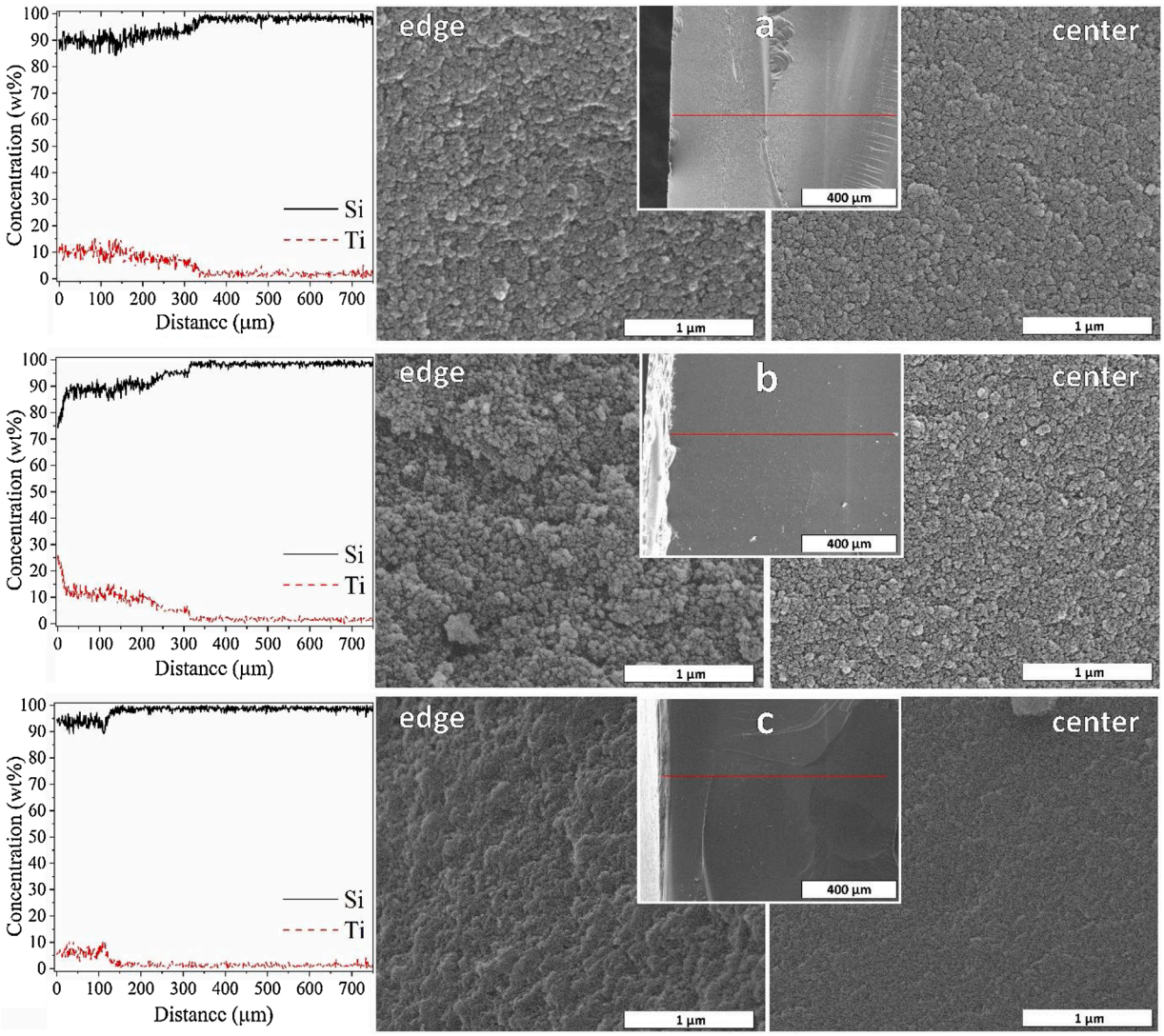

Fig. 4. EDS line analysis and the cross-sectional view taken from the edge and the center of the freshly fractured surfaces for **(a)** TiPG, **(b)** TiPG-AL, and **(c)** TiPG-HT.

the mesoporous range further increased but, some of the micropores diminished probably due to particle and/or surface dissolution of silica clusters [33]. Such alterations caused a reduction in the SSA but, as expected enhanced the Vp. The sequential heat treatment of initially produced PG caused both the compaction of silica particles (clusters) and the shrinkage of the liquation channels due to softening of the silica skeleton. Thus, after the heat treatment, the pores collapsed to certain degree, causing SSA and V_P to decrease. The TiO_2 crystallization on the pore walls and struts correspondingly resulted in a reduction of both SSA (to 282.9 m^2/g) and Vp (to 0.277 cm^3/g).

The XRD pattern of the TiO_2 powder synthesized, as shown in Fig. 2 **(a),** suggests that the material is phase pure anatase TiO_2 (PDF #00-021-1272). The mean crystallite size (D) as calculated by using the Debye–Scherrer formula was 36.2 nm that was akin to the values reported by other researchers [34,35]. For crystallite size calculations, full-width at half maximum (FWHM) for the most intense peak for the anatase TiO_2 at 2θ of 25.3°, belonging to (101), was considered. A visible but weak diffraction peak at 2θ of 25.3° in the XRD patterns of TiPGs, suggests the presence of TiO_2 crystallites. The same diffraction peak became pronounced for the twice Ti impregnated PG (Tix2PG), similar to the findings of Anpo et al. [36].

The FTIR spectra for SBG, PG, TiPG, and TiO_2 powder are shown in Fig. 2**(b)**. It is difficult to resolve each infrared band due to overlapping of the bands detected from several bonds in the glass network and TiO_2 powder. The bands at ~450, ~800, and ~1080 cm^{-1} are assigned to Si–O–Si bonds [37–39] though those at ~920 and ~670 cm^{-1} (with shoulder at ~695 cm^{-1}) correspond to Si—O—B bonds [40–42]. Moreover, there were the B–O stretching vibration bands at ~880, ~980, ~1370 and ~1280 cm^{-1} [43,44]. After acid leaching, the bands associated with B–O and Si—O—B bonds either decreased in the intensity or completely disappeared. In addition, the intensity of the bands belonging to Si—O—Si bonds increased, implying that the initially generated alkali-borate phase was removed by the acid leaching and the remaining porous structure mostly consists of silica. The FTIR spectrum of PG is highly compatible with that of the previously reported [32,42]. The dominant band centered at ~438 cm^{-1} in the spectrum of TiO_2 powder is assigned to Ti—O—Ti bonds in crystalline TiO_2 structure [45,46]. The bands for the Ti—O—Ti and Si—O—Ti bonds (at 960 cm^{-1}) [47,48] were not detected due to the overlapping with the other bands.

SEM images taken from the surfaces of TiPG, Tix2PG, TiPG-AL, and TiPG-HT are shown in Fig. 3. The characteristic “worm-like” pore structure (see also the inset in Fig. 3**(a)** for the observed pore morphology) developed in PGs was actually coming from spinodal decomposition [49,50]. When twice impregnation was applied, a higher surface coverage was obtained (Fig. 3**(b)**). Instead, for alkaline treated sample (TiPG-AL) no clear cellular structure but a very rough surface, possibly due to the deformation of the silica skeleton was observed (Fig. 3**(c)**). Previous studies [20,51,52] revealed that during a heat

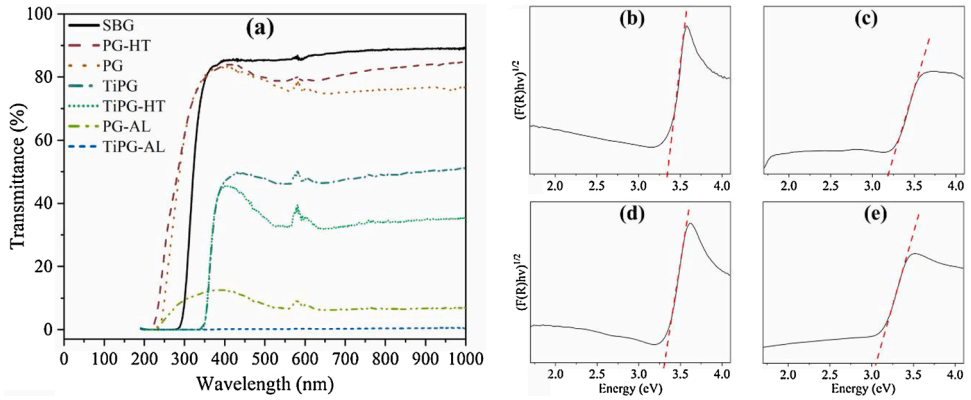

Fig. 5. **(a)** The transmittance spectra of the investigated glasses, and Kubelka-Munk transformed reflectance graphs (Tauc plots) for **(b)** TiPG, **(c)** TiPG-AL, **(d)** TiPG-HT, and **(e)** TiO_2 powder.

treatment procedure, the migration of B atoms to surface increases the surface acidity. This promotes the polymerization of Ti-O-Ti species and enhances the Ti crystallization [53]. However, since in the current study no TiO_2 related peaks were seen in the XRD pattern for TiPG-HT, the observed morphological elevation was related to the sintering shrinkage, see Fig. 3**(d)**.

Fig. 4 shows the SEM images and EDS line analysis taken from the edge (close to the surface) and the center of the freshly fractured surfaces for TiPG, TiPG-AL, and TiPG-HT. The EDS line analysis was performed on the cross-section up to a depth of ~750 μm. Data were given in the insets of Fig. 4 for each TiPG. The EDS peaks for SiKα and TiKα were converted to ZAF corrected (an intensity correction applied by the instrument, which is related to the atomic number (Z), absorption (A) and fluorescence (F) effects) weight percentage to get information on the penetration depth of Ti. An abrupt decrease in Ti concentration at a depth of ~330 μm from the surface (see Fig. 4**(a)**) is attributed to insufficient impregnation of the Ti solution due to hindrance of the silica clusters in the pores, or hampered hydrolysis reactions. Yamashita et al. [16] anchored Ti into a PG by metal ion implantation and reported similar results stating that Ti concentration was higher in the surface region at a depth of ~40 nm. The concentration of Ti in the near-surface region of TiPG-AL was about twice more than that of TiPG but, gradually decreased toward the interior as shown in Fig. 4**(b)**. This was expected since the surface of TiPG-AL contains larger pores (and much lower silica clusters) facilitating the infiltration of the Ti solution into the glass structure. For TiPG-HT, the shrinkage related narrowing of the pores caused a reduction of the Ti penetration hence, the Ti-rich layer depth was only around 150 μm, as seen in Fig. 4**(c)**.

Fig. 5**(a)** shows the transmittance spectra of SBG, PGs, and TiPGs. Precise determination of the optical properties of a PG is quite difficult since it has complex structure including different substances with dissimilar refractive indices. The size and volume of the liquation channels, amount and packing of the silica clusters in the channels affect the transparency of the glass [54–56]. Removal of Na ions from the structure and elimination of the atoms that cause UV absorption even in small amounts are thought to be the reasons for the shift of the absorption edge of PGs toward lower wavelength with respect to SBG. Phase separation followed by acid leaching is one of the commonly practiced processes to obtain UV transparent glass [57,58]. The visible region transparency of SBG decreased from ~85 % to ~75 % as a result of acid leaching process due to the generation of new pores. The pores act as Rayleigh scattering points since the average pore size in PGs and TiPGs is less than 22 nm, that is smaller than the wavelength of the incident light. Antropova and Drozdova [59] reported that turbidity and light transmittance decreased with increasing pore size. In this regard, the distinct decrease in the transparency of PG-AL by ~10 % was attributed both to the increase in pore size and to the partial erosion of the silica skeleton by alkaline leaching causing enhanced surface roughness. The TiO_2 crystallites developed within or on the surface of PGs caused scattering hence decreased the transparency [36]. The absorption edge of PG at ~225 nm shifted to ~340−370 nm upon TiO_2 embedding. The adsorption edge at 370−380 nm was assigned to the intrinsic band gap absorption of anatase TiO_2 corroborating the presence of such phase [60,61].

Table 1
The values (mean ave. ± standard deviation) for the band gap energy, MB adsorption in the dark, and MB removal efficiency under UV for TiPG, TiPG-AL, TiPG-HT, and TiO_2 powder.

Sample	Band gap (eV)	MB dark adsorption (%)	MB removal under UV Light (%)
TiPG	3.35 ± 0.02	60.25 ± 3.56	91.65 ± 3.80
TiPG-AL	3.19 ± 0.02	93.53 ± 3.86	> 99.00
TiPG-HT	3.31 ± 0.05	54.88 ± 3.62	86.49 ± 2.72
TiO_2 powder	3.05 ± 0.01	7.66 ± 1.91	32.36 ± 1.88

Kubelka-Munk transformed reflectance graphs (Tauc plots) for TiPG, TiPG-AL, TiPG-HT, and TiO_2 powder are shown in Fig. 5**(b–e),** and the indirect optical band gap (Eg) values extracted from the plots were listed in Table 1. The Eg value of the synthesized anatase TiO_2 powder was measured as 3.05 eV, akin to the acceptable values [62,63]. The higher Eg value of TiPG relative to TiO_2 powder implies that the size of the TiO_2 crystallites developed in and on the pore surfaces and struts of PGs was smaller than that of the synthesized TiO_2 powder. It is known that Eg increases as the particle size decreases due to the quantum size effect [30,34,64]. For example, Jiang et al. [8] showed that TiO_2 including porous supports had Eg values between 3.1–3.5 eV that decreased with increasing TiO_2 loading rate. Besides, the development of fine porous structure inhibits the agglomeration tendency of the TiO_2 particles trapped in the pores, i.e. basically the pore size defines the boundary conditions for the growth, resulting in enhanced Eg as compared to those of non-porous substrates [18,64].

3.2. *MB decolorization*

MB decolorization tests were performed independently in the dark and under a UV light source. The difference in the MB removal efficiency between these two tests was credited to the photocatalytic degradation effect of TiO_2 crystallites embedded within the PG. Fig. 6**(a)** shows the variation of the MB removal efficiency with respect to time in the dark, i.e. dark adsorption for all glasses investigated. The SSA of PG-AL was the lowest among all the glasses tested. However, it showed the highest MB adsorption capability. This information suggests that the SSA was not the principle contributing factor for the adsorption of MB in the PGs. Previous studies concluded that PG has high adsorption capability

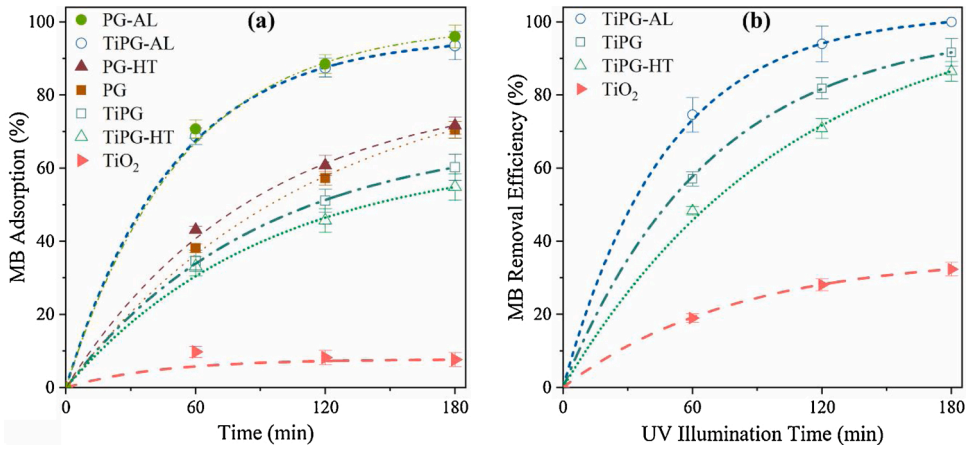

Fig. 6. (a) MB adsorption capacity in the dark with time for PG, PG-AL, PG-HT, TiPG, TiPG-AL, TiPG-HT, and TiO_2 powder; and **(b)** Variation of the MB removal efficiency under UV light with illumination time for TiPG, TiPG-AL, TiPG-HT, and TiO_2 powder.

because of its relatively high SSA, V_P, and negatively charged surface silanol groups [20,65]. Being a cationic dye, MB molecules are attracted by the negatively charged glass surfaces [66]. Removing the silica clusters by alkaline leaching facilitated the penetration of the aqueous MB solution through the porous structure [17,67,68], and altered the surface functionality, i.e. increased the surface adsorption sites causing an enhanced capacity.

Fig. 6**(b)** demonstrates the MB removal efficiency under UV light at the end of the 3 h of test. The data are summarized also in Table 1. The TiPGs exhibited better MB removal efficiency (reaching even to complete removal capacity for TiPG-AL) than the TiO_2 powder synthesized. Similar results have been reported previously in other studies [8,9,18,64]. Such favorable total removal efficiency of PG embedded with TiO_2 can be related to a combination of some factors such as the intrinsic higher reactivity due to homogenously dispersed TiO_2 nano-crystallites in the fine pore (<30 nm) structure [69], the increase of Eg due to smaller crystal size [8,36,64], reduction of charge recombination (electron-hole pair), i.e. small pore wall thickness providing a shorter distance for the transfer of the photogenerated electrons and holes to the surface [70], and the glass transparency promoting higher amount of excited TiO_2 compared to those of non-transparent host materials [17].

4. Conclusions

Porous glasses (PGs) with various pore architectures are produced from ordinary sodium borosilicate glasses. The porous substrates are effectively infiltrated with a titanium precursor. The anatase TiO_2 is crystallized in the pore and strut surfaces of the Ti infiltrated PG by successive heat treatment. PGs having relatively high specific surface area of 358 m^2/g, still maintains the 3D interconnected porosity with a specific surface area of 282.9 m^2/g upon TiO_2 crystallization while their transparency in visible region decreases from ~75 % to ~48 %. Methylene blue (MB) removal tests reveal that TiO_2 embedded PG (TiPGs) exhibit high MB adsorption capability in the dark and MB removal efficiency under UV illumination. While the MB dark adsorption was around 70 % for PG, the efficiency of ~ 92 % for TiO_2 embedded PG (TiPG), and virtually complete removal for alkaline leached TiO_2 embedded PG (TiPG-AL) was observed under UV illumination in the 3 h period. TiO_2 embedded highly porous glasses demonstrate both powerful adsorption capability and photocatalytic ability, i.e. a synergic purification effect, than the anatase TiO_2 powder. Such glasses can be practically used for water purification and indoor air filtration for the removal of volatile organic compounds.

Declaration of Competing Interest

All the authors declare that there is no conflict of interest.

Acknowledgments

This study is dedicated to the memory of Professor Dr. Muharrem Timucin who was our mentor, teacher, inspiration, and a well-recognized, brilliant scientist. The authors thank Middle East Technical University for the partial financial support through project number BAP-03-08-2016-004. Cekdar Vakif Ahmetoglu acknowledges the support of the Alexander von Humboldt (AvH) Foundation.

References

[1] K. Hashimoto, H. Irie, A. Fujishima, TiO_2 photocatalysis: a historical overview and future prospects, Jpn. J. Appl. Phys. 44 (12R) (2005) 8269–8285.
[2] D. Bahnemann, Photocatalytic water treatment: solar energy applications, Sol. Energy 77 (5) (2004) 445–459.
[3] J. Schneider, M. Matsuoka, M. Takeuchi, J. Zhang, Y. Horiuchi, M. Anpo, D. W. Bahnemann, Understanding TiO_2 photocatalysis: mechanisms and materials, Chem. Rev. 114 (19) (2014) 9919–9986.
[4] G. Li, L. Lv, H. Fan, J. Ma, Y. Li, Y. Wan, X. Zhao, Effect of the agglomeration of TiO2 nanoparticles on their photocatalytic performance in the aqueous phase, J. Colloid Interface Sci. 348 (2) (2010) 342–347.
[5] X. Weimin, S.-u. Geissen, Separation of titanium dioxide from photocatalytically treated water by cross-flow microfiltration, Water Res. 35 (5) (2001) 1256–1262.
[6] J. Byrne, B. Eggins, N. Brown, B. McKinney, M. Rouse, Immobilisation of TiO_2 powder for the treatment of polluted water, Appl. Catal. B 17 (1-2) (1998) 25–36.
[7] R.L. Pozzo, M.A. Baltanas, A.E. Cassano, Supported titanium oxide as photocatalyst in water decontamination: state of the art, Catal. Today 39 (3) (1997) 219–231.
[8] C. Jiang, K.Y. Lee, C.M. Parlett, M.K. Bayazit, C.C. Lau, Q. Ruan, S.J. Moniz, A. F. Lee, J. Tang, Size-controlled TiO_2 nanoparticles on porous hosts for enhanced photocatalytic hydrogen production, Appl. Catal. A Gen. 521 (2016) 133–139.
[9] X.-j. Wang, F.-t. Li, Y.-j. Hao, S.-j. Liu, M.-l. Yang, TiO_2/SBA-15 composites prepared using H_2TiO_3 by hydrothermal method and its photocatalytic activity, Mater. Lett. 99 (2013) 38–41.
[10] Y. Kuwahara, K. Maki, Y. Matsumura, T. Kamegawa, K. Mori, H. Yamashita, Hydrophobic modification of a mesoporous silica surface using a fluorine-containing silylation agent and its application as an advantageous host material for the TiO_2 photocatalyst, J. Phys. Chem. C 113 (4) (2009) 1552–1559.
[11] Y. Dong, D. Tang, C. Li, Photocatalytic oxidation of methyl orange in water phase by immobilized TiO_2-carbon nanotube nanocomposite photocatalyst, Appl. Surf. Sci. 296 (2014) 1–7.
[12] C.H. Kim, B.-H. Kim, K.S. Yang, TiO_2 nanoparticles loaded on graphene/carbon composite nanofibers by electrospinning for increased photocatalysis, Carbon 50 (7) (2012) 2472–2481.
[13] T. Zou, C. Xie, Y. Liu, S. Zhang, Z. Zou, S. Zhang, Full mineralization of toluene by photocatalytic degradation with porous TiO_2/SiC nanocomposite film, J. Alloys. Compd. 552 (2013) 504–510.
[14] D. Hao, Z. Yang, C. Jiang, J. Zhang, Synergistic photocatalytic effect of TiO_2 coatings and p-type semiconductive SiC foam supports for degradation of organic contaminant, Appl. Catal. B 144 (2014) 196–202.
[15] K. Kato, Photocatalytic property of TiO_2 anchored on porous alumina ceramic support by the alkoxide method, J. Ceram. Soc. Jpn. 101 (1171) (1993) 245–249.

[16] H. Yamashita, M. Honda, M. Harada, Y. Ichihashi, M. Anpo, T. Hirao, N. Itoh, N. Iwamoto, Preparation of titanium oxide photocatalysts anchored on porous silica glass by a metal ion-implantation method and their photocatalytic reactivities for the degradation of 2-propanol diluted in water, J. Phys. Chem. B 102 (52) (1998) 10707–10711.

[17] T. Yazawa, F. Machida, N. Kubo, T. Jin, Photocatalytic activity of transparent porous glass supported TiO_2, Ceram. Int. 35 (8) (2009) 3321–3325.

[18] I. Mazali, A. Souza Filho, B. Viana, J. Mendes Filho, O. Alves, Size-controllable synthesis of nanosized-TiO_2 anatase using porous Vycor glass as template, J. Nanoparticle Res. 8 (1) (2006) 141–148.

[19] D. Enke, F. Janowski, W. Schwieger, Porous glasses in the 21st century—a short review, Microporous Mesoporous Mater. 60 (1-3) (2003) 19–30.

[20] F. Schüth, K.S.W. Sing, J. Weitkamp, Handbook of Porous Solids, Wiley-Vch, 2002.

[21] M.E. Nordberg, Properties of some Vycor-brand glasses, J. Am. Ceram. Soc. 27 (10) (1944) 299–305.

[22] T.H. Elmer, Porous and Reconstructed Glasses, 4, ASM International, Engineered Materials Handbook, 1991, pp. 427–432.

[23] C. Vakifahmetoglu, T. Semerci, G.D. Soraru, Closed porosity ceramics and glasses, J. Am. Ceram. Soc. 103 (5) (2020) 2941–2969.

[24] C. Vakifahmetoglu, D. Zeydanli, V.C. Ozalp, B.A. Borsa, G.D. Soraru, Hierarchically porous polymer derived ceramics: a promising platform for multidrug delivery systems, Mater. Des. 140 (2018) 37–44.

[25] A. Kuznetsova, A. Volkova, L. Ermakova, T. Antropova, Iron (III) ion adsorption on macroporous glass, Glass Phys. Chem. 44 (1) (2018) 41–46.

[26] S. Yanagida, K. Hirayama, K. Iwasaki, A. Yasumori, Adsorption and photocatalytic decomposition of gaseous 2-propanol using TiO_2-coated porous glass fiber cloth, Catalysts 9 (1) (2019) 82.

[27] E. Aubry, M.N. Ghazzal, V. Demange, N. Chaoui, D. Robert, A. Billard, Poisoning prevention of TiO_2 photocatalyst coatings sputtered on soda-lime glass by intercalation of SiNx diffusion barriers, Surf. Coat. Technol. 201 (18) (2007) 7706–7712.

[28] E.B. Ertuş, C. Vakifahmetoglu, A. Öztürk, Production and properties of phase separated porous glass, Ceram. Int. 46 (4) (2020) 4947–4951.

[29] M. Thommes, K. Kaneko, A.V. Neimark, J.P. Olivier, F. Rodriguez-Reinoso, J. Rouquerol, K.S. Sing, Physisorption of gases, with special reference to the evaluation of surface area and pore size distribution (IUPAC Technical Report), Pure Appl. Chem. 87 (9-10) (2015) 1051–1069.

[30] R. López, R. Gómez, Band-gap energy estimation from diffuse reflectance measurements on sol–gel and commercial TiO_2: a comparative study, J. Solgel Sci. Technol. 61 (1) (2012) 1–7.

[31] V. Kreisberg, V. Rakcheev, T. Antropova, Influence of the acid concentration on the morphology of micropores and mesopores in porous glasses, Glass Phys. Chem. 32 (6) (2006) 615–622.

[32] G. Toquer, C. Delchet, M. Nemec, A. Grandjean, Effect of leaching concentration and time on the morphology of pores in porous glasses, J. Non-cryst. Solids 357 (6) (2011) 1552–1557.

[33] M. Lyubavin, T. Burkat, V. Pak, Fabrication of silica membranes with controlled pore structure, Inorg. Mater. 44 (2) (2008) 203–206.

[34] G.S. Pozan, A. Kambur, Effect of operating parameters and titanium source on photodegradation of phenol, Indian J. Chem. Technol. 21 (2014) 272–279.

[35] H. Soni, J.N. Kumar, K. Patel, R.N. Kumar, Photocatalytic decoloration of three commercial dyes in aqueous phase and industrial effluents using TiO_2 nanoparticles, Desalin. Water Treat. 57 (14) (2016) 6355–6364.

[36] M. Anpo, N. Aikawa, Y. Kubokawa, M. Che, C. Louis, E. Giamello, Photoluminescence and photocatalytic activity of highly dispersed titanium oxide anchored onto porous Vycor glass, J. Phys. Chem. 89 (23) (1985) 5017–5021.

[37] M. Hasanuzzaman, M. Sajjia, A. Rafferty, A.-G. Olabi, Thermal behaviour of zircon/zirconia-added chemically durable borosilicate porous glass, Thermochim. Acta 555 (2013) 81–88.

[38] H. Darwish, M. Gomaa, Effect of compositional changes on the structure and properties of alkali-alumino borosilicate glasses, J. Mater. Sci. Mater. Electron. 17 (1) (2006) 35–42.

[39] K. El-Egili, Infrared studies of Na_2O–B_2O_3–SiO_2 and Al_2O_3–Na_2O–B_2O_3–SiO_2 glasses, Phys. B Condens. Matter 325 (2003) 340–348.

[40] M. Nolan, T. Perova, R. Moore, C. Beitia, J. McGilp, H. Gamble, Spectroscopic investigations of borosilicate glass and its application as a dopant source for shallow junctions, J. Electrochem. Soc. 147 (8) (2000) 3100–3105.

[41] Z.-x. Hou, S.-h. Wang, Z.-l. Xue, H.-r. Lu, C.-l. Niu, H. Wang, B. Sun, C. Su, Crystallization and microstructural characterization of B_2O_3–Al_2O_3–SiO_2 glass, J. Non. Solids 356 (4-5) (2010) 201–207.

[42] M.A. Mazo, J. Sanguino, A. Tamayo, J. Rubio, Carbon nanofibers grown in situ on porous glass, J. Nano Res. 50 (2017) 1–17.

[43] L. Balachander, G. Ramadevudu, M. Shareefuddin, R. Sayanna, Y. Venudhar, IR analysis of borate glasses containing three alkali oxides, ScienceAsia 39 (2) (2013) 278–283.

[44] X. Zhu, C. Mai, M. Li, Effects of B_2O_3 content variation on the Bi ions in Bi_2O_3–B_2O_3–SiO_2 glass structure, J. Non. Solids 388 (2014) 55–61.

[45] H. Kawamura, S. Okuto, S. Taruta, N. Takusagawa, K. Kitajima, Inhomogeneous distribution of TiO_2 in porous glass specimen anchored by impregnation method using aqueous solutions, J. Ceram. Soc. Jpn. 104 (1216) (1996) 1160–1162.

[46] J.-Y. Zhang, I.W. Boyd, B. O'sullivan, P. Hurley, P. Kelly, J.-P. Senateur, Nanocrystalline TiO_2 films studied by optical, XRD and FTIR spectroscopy, J. Non. Solids 303 (1) (2002) 134–138.

[47] A. Mirabedini, S. Mirabedini, A. Babalou, S. Pazokifard, Synthesis, characterization and enhanced photocatalytic activity of TiO_2/SiO_2 nanocomposite in an aqueous solution and acrylic-based coatings, Prog. Org. Coat. 72 (3) (2011) 453–460.

[48] S. Rasalingam, R. Peng, R.T. Koodali, Removal of hazardous pollutants from wastewaters: applications of TiO_2-SiO_2 mixed oxide materials, J. Nanomater. 2014 (2014) 1–10.

[49] D. Enke, F. Janowski, W. Gille, W. Schwieger, Structure and texture analysis of colloidal silica in porous glasses, Colloids Surf. A Physicochem. Eng. Asp. 187 (2001) 131–139.

[50] T. Elmer, M. Nordberg, G. Carrier, E. Korda, Phase separation in borosilicate glasses as seen by electron microscopy and scanning electron microscopy, J. Am. Ceram. Soc. 53 (4) (1970) 171–175.

[51] A. Dawidowicz, Controlled Porosity Glasses (CPGs) As Adsorbents, Molecular Sieves, Ion-exchangers and Support Materials, Studies in Surface Science and Catalysis, Elsevier, 1996, pp. 31–56.

[52] T.H. Elmer, I.D. Chapman, M.E. Nordberg, Changes in length and infrared transmittance during thermal dehydration of porous glass at temperatures up to 1200°, J. Phys. Chem. 66 (8) (1962) 1517–1519.

[53] M.A. Behnajady, H. Eskandarloo, N. Modirshahla, M. Shokri, Sol-gel low-temperature synthesis of stable anatase-type TiO_2 nanoparticles under different conditions and its photocatalytic activity, Photochem. Photobiol. 87 (5) (2011) 1002–1008.

[54] T. Antropova, I. Anfimova, G. Golovina, Influence of the composition and temperature of heat treatment of porous glasses on their structure and light transmission in the visible spectral range, Glass Phys. Chem. 35 (6) (2009) 572–579.

[55] T.V. Antropova, I.N. Anfimova, The influence of thermal treatment of the porous glass plates on the character of their scattering in visible spectral region, Opt. Appl. 40 (2) (2010) 285.

[56] S. Ogawa, $1/\lambda^4$ scattering of light during the drying process in porous Vycor glass with nano-sized pores, JOSA A 30 (2) (2013) 154–159.

[57] M. Nordberg, Ultraviolet-transmitting glasses for mercury-vapor lamps, J. Am. Ceram. Soc. 30 (6) (1947) 174–179.

[58] N.M. Emery, Method of making ultraviolet transmitting high silica glass, Google Patents, 1950.

[59] T.V. Antropova, I. Drozdova, Sintering of optical porous glasses, Opt. Appl. 33 (1) (2002) 13–22.

[60] R. Poliah, S. Sreekantan, Characterization and photocatalytic activity of enhanced copper-silica-loaded titania prepared via hydrothermal method, J. Nanomater. 2011 (2011) 58–67.

[61] J. Yu, X. Zhao, Q. Zhao, G. Wang, Preparation and characterization of super-hydrophilic porous TiO_2 coating films, Mater. Chem. Phys. 68 (1-3) (2001) 253–259.

[62] L. Agartan, D. Kapusuz, J. Park, A. Ozturk, Effect of initial water content and calcination temperature on photocatalytic properties of TiO_2 nanopowders synthesized by the sol–gel process, Ceram. Int. 41 (10) (2015) 12788–12797.

[63] K. Kočí, L. Obalová, L. Matějová, D. Plachá, Z. Lacný, J. Jirkovský, O. Šolcová, Effect of TiO_2 particle size on the photocatalytic reduction of CO_2, Appl. Catal. B 89 (3-4) (2009) 494–502.

[64] C. Shen, Y. Wang, J. Xu, G. Luo, Facile synthesis and photocatalytic properties of TiO_2 nanoparticles supported on porous glass beads, Chem. Eng. J. 209 (2012) 478–485.

[65] T. Mizutani, A. Mizutani, Adsorption of cationic biological materials on controlled pore glass, Anal. Biochem. 83 (1) (1977) 216–221.

[66] D. Zeydanli, S. Akman, C. Vakifahmetoglu, Polymer-derived ceramic adsorbent for pollutant removal from water, J. Am. Ceram. Soc. 101 (6) (2018) 2258–2265.

[67] R. Müller, N. Anders, J. Titus, D. Enke, Ultra-thin porous glass membranes—an innovative material for the immobilization of active species for optical chemosensors, Talanta 107 (2013) 255–262.

[68] S. Lei, J.-i. Miyamoto, H. Kanoh, Y. Nakahigashi, K. Kaneko, Enhancement of the methylene blue adsorption rate for ultramicroporous carbon fiber by addition of mesopores, Carbon 44 (10) (2006) 1884–1890.

[69] Y. Acosta-Silva, R. Nava, V. Hernández-Morales, S. Macías-Sánchez, M. Gómez-Herrera, B. Pawelec, Methylene blue photodegradation over titania-decorated SBA-15, Appl. Catal. B 110 (2011) 108–117.

[70] X. Chen, S. Shen, L. Guo, S.S. Mao, Semiconductor-based photocatalytic hydrogen generation, Chem. Rev. 110 (11) (2010) 6503–6570.